Analyst

www.rsc.org/analyst

Volume 137 | Number 18 | 21 September 2012 | Pages 4095–4376

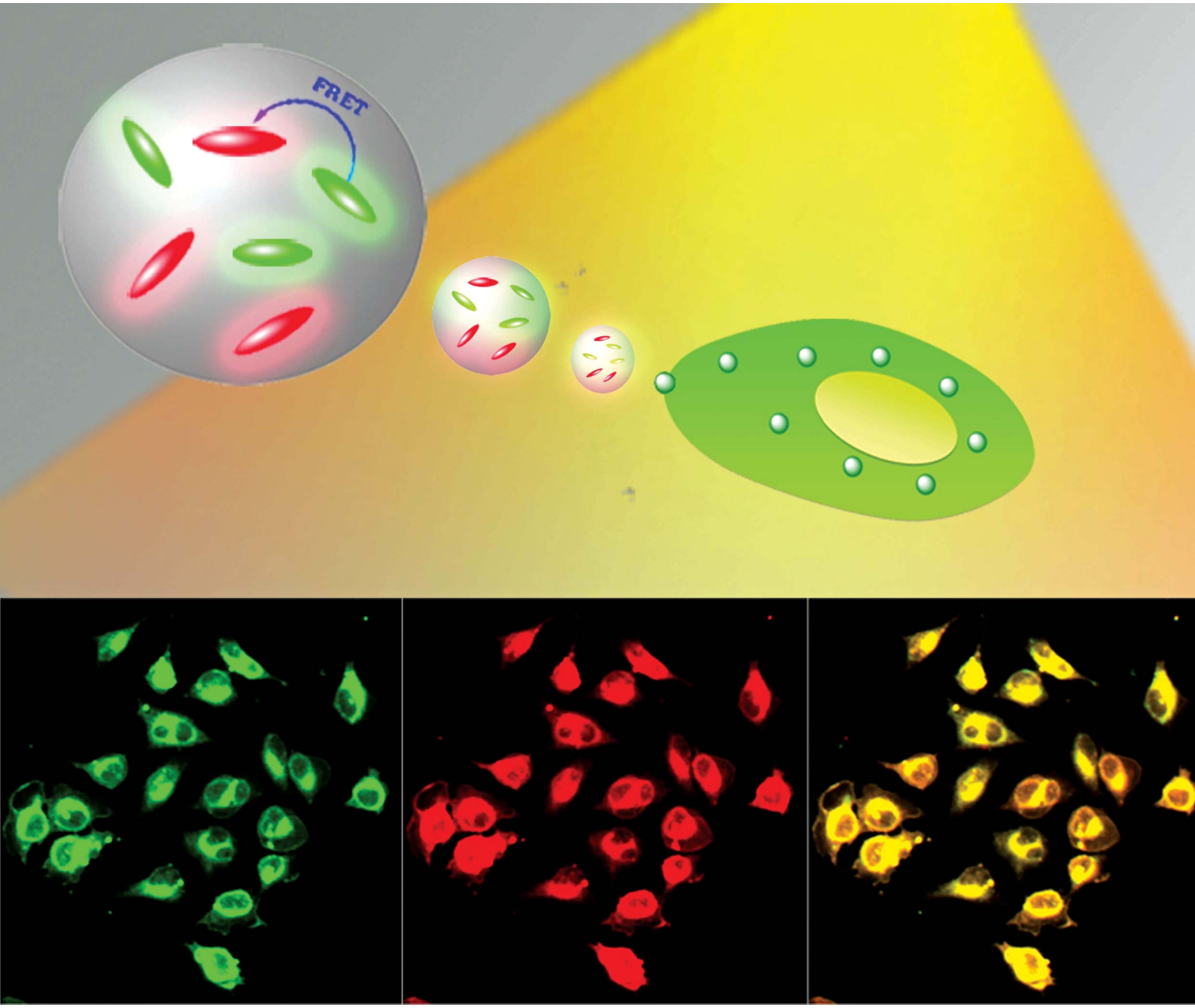

ISSN 0003-2654

HOT ARTICLE

Qingdong Zheng *et al.*

Silylated BODIPY dyes and their use in dye-encapsulated silica nanoparticles with switchable emitting wavelengths for cellular imaging

RSC Publishing

0003-2654(2012)137:18;1-Z

Analyst

Dynamic Article Links

Cite this: *Analyst*, 2012, **137**, 4140

www.rsc.org/analyst

PAPER

Silylated BODIPY dyes and their use in dye-encapsulated silica nanoparticles with switchable emitting wavelengths for cellular imaging

Xuehua Hong,[ab] Zhuyuan Wang,[c] Jing Yang,[c] Qingdong Zheng,*[a] Shenfei Zong,[c] Yu Sheng,[b] Deqin Zhu,[b] Changquan Tang[a] and Yiping Cui[c]

Received 22nd March 2012, Accepted 11th June 2012
DOI: 10.1039/c2an35389j

Two silylated BODIPY derivatives were synthesized, characterized and used for the fabrication of the dye-encapsulated silica nanoparticles. The fluorophores were covalently incorporated into the silica matrix to minimize any fluorophore leakage. The synthesized fluorophore-doped nanoparticles were stable in aqueous solution and monodisperse with diameters of 20–25 nm. By incorporating the two BODIPY dyes simultaneously at a controlled ratio, silica nanoparticles with switchable emitting wavelengths were achieved with a change in the excitation wavelength. Thus by using the dual-fluorophore-doped nanoparticles, two-color imaging was demonstrated with minimal background signal by employing an appropriate excitation light source and appropriate excitation/emission filter sets. Further, the surfaces of the dual-fluorophore-doped nanoparticles were functionalized with folic acid to allow for the recognition of HeLa cells which over-express the folate receptors.

Introduction

Dipyrromethene boron difluoride (BODIPY) dyes were first known as efficient lasing dyes more than two decades ago due to their high fluorescence quantum yields, intense absorption and high lasing efficiencies.[1–3] With the development of biomedical imaging and therapy, recent years have witnessed increasing efforts made on the design and synthesis of functionalized BODIPY derivatives with various prominent properties.[2–5] In biological applications, long-wavelength imaging probes are of great importance in order to reduce background fluorescence as well as to penetrate into deep tissues.[6] BODIPY dyes with red-shifted emission can be either achieved by increasing the conjugation length of the BODIPY core or by introducing strong electron acceptors into the BODIPY core.[2,3,7–9] The former method might lead to a decreased solubility of the targeted fluorophore in aqueous solution, whereas the latter one might lead to reduced fluorescence quantum yields. However, some less water soluble BODIPY probes can be made more biocompatible by being placed inside a nanocarrier. In this way, the circulation time of the probes may be controlled by the size of the nanocarrier. At the same time, the brightness per particle is greatly enhanced over single molecule delivery because a single 50 nm particle may carry several thousand dye molecules.[10] Furthermore, probes with different functionalities can be realized with ease by surface modification of the nanocarrier. We noticed that the introduction of some water soluble groups such as poly-(ethylene glycol)s may also be used to increase the solubility of the BODIPY dyes.[8] But it always complicates the synthetic procedure, especially when other biological groups such as folic acid or transferrin are needed to be conjugated to the BODIPY dye. Thus, in the biological imaging application, BODIPY-doped nanoparticles show a number of advantages such as amplified signal intensities, and reduced photobleaching.[11,12] Besides the biological imaging application, fluorescence nanoparticle probes are also very feasible for biomarker and immunoassay applications.[13–15] Moreover, the fluorescence nanoparticles can be easily fabricated as multiplexed optical probes which can diagnose multiple bioassays simultaneously, simplify the testing process and shorten the detection time.[16,17] By using the multiplexed probe, one can even envision a dynamic, multicolor, co-localization methodology to follow proteins, nucleic acids, molecular machines, and assemblies within living biosystems.[18] As a matrix material for fluorophores, silica nanoparticles exhibit good biocompatibility, and they are particularly useful for medical imaging and targeted drug delivery because they are assumed to be relatively inert and non-toxic when compared to other nanomaterials (*e.g.*, CdSe quantum dots, CdTe quantum dots, and other metal-based nanoparticles).[10] In addition, they can be manufactured in a range of sizes and their surfaces can be modified for specific biological applications by introducing functional groups that inhibit particle aggregation and promote their uptake

[a]*State Key Laboratory of Structural Chemistry, Fujian Institute of Research on the Structure of Matter, Chinese Academy of Sciences, Fuzhou, 350002, P. R. China. E-mail: qingdongzheng@fjirsm.ac.cn; Fax: +86-591-83721625*
[b]*School of Materials Science and Engineering, Fujian Normal University, Fuzhou, 350007 P. R. China*
[c]*Advanced Photonics Center, Southeast University, Nanjing 210096, P. R. China*

into cells, or their binding to specific macromolecular receptors, or the delivery of therapeutic agents.

Although many BODIPY dyes have been designed and prepared for various biological applications, relatively few silylated BODIPY dyes as well as the corresponding dye-doped silica nanoparticles have been reported.[19] Here, we report on the synthesis and characterization of two silylated BODIPY dyes and their use in dye-encapsulated silica nanoparticles with switchable emitting wavelengths for cellular imaging. With the aid of the silylated functional group, BODIPY dyes can be covalently incorporated into the silica nanoparticles using the oil-in-water method. Furthermore, to realize multiplexed imaging, we doped two different dyes into the same nanoparticle, which is able to emit light with different colors based on a change in excitation wavelengths. Furthermore, the surfaces of nanoparticles were functionalized with folic acid (FA) to endow the targeting ability of the nanoparticles.

Results and discussion

Synthesis and optical properties of silylated BODIPY dyes

The synthetic routes to the silylated BODIPY dyes **1** and **2** were depicted in Scheme 1. The key intermediates in the synthesis are the BODIPY dyes with carboxylic acid ester groups (**5** and **6**), which were prepared by reacting the corresponding benzaldehydes with 2,4-dimethylpyrrole in the presence of trifluoroacetic acid (TFA) and 2,3-dichloro-5,6-dicyano-1,4-benzoquinone (DDQ), followed by an addition of $BF_3 \cdot OEt_2$. Then, a Knoevenagel-type condensation reaction between compound **6** and *p*-methoxybenzaldehyde in the presence of piperidine and acetic acid afforded compound **8** in 26% yield. Hydrolysis of compounds **5** and **8** under alkaline conditions afforded compounds **7** and **9** in yields of 95% and 90%, respectively. The carboxyl group of compound **7** was activated by reacting with *N*-hydroxysuccinimide (NHS), and the resulting product was reacted with (3-aminopropyl)triethoxysilane (APTES) to afford dye **1** in 77%. Under the same reaction condition, dye **2** was synthesized from compound **9** with a yield of 65%. All new compounds were characterized by ^{1}H NMR and HRMS, and the purity of the target dyes **1** and **2** was further confirmed by elemental analysis.

Linear absorption and emission spectra of silylated BODIPY dyes (**1** and **2**) were investigated in toluene at room temperature (as shown in Fig. 1). Dye **1** has a linear absorption maximum at 504 nm and an emission maximum at 517 nm. The linear absorption maximum of dye **2** is around 650 nm, and the emission peak is at 667 nm. The introduction of two extra styryl groups to the BODIPY core leads to *ca.* 150 nm red-shifted linear absorption and emission bands. Red-shifted dyes have an advantage in bioassay and cellular imaging applications since light in this region is less absorbed and scattered by tissues, which enables a deeper light penetration as well as a better signal-to-noise ratio by minimal interference from the background autofluorescence.[20] Similar to other BODIPY dyes, dye **1** and dye **2** are highly fluorescent with fluorescence quantum yields of 0.75 and 0.52, respectively. We noticed that dyes **1** and **2** have relatively small Stokes shifts of around 13 nm and 17 nm respectively, in agreement with most reported BODIPY dyes.[2,3]

Synthesis, structural and optical properties of dye-doped nanoparticles

The dye-doped nanoparticles were prepared by the co-hydrolysis and polycondensation of the individual silylated BODIPY dyes and triethoxyvinysilane (VTES) within the non-polar core of an oil-in-water microemulsion. The successful doping of the dyes into nanoparticles was verified by the absorption and emission spectra of the resulting silica nanoparticles. The surfaces of nanoparticles were functionalized with amino groups, which were further conjugated with FA by an amination reaction.

To demonstrate whether or not the BODIPY dyes were covalently incorporated into nanoparticles rather than merely physically encapsulated, thin layer chromatography (TLC) was performed on silica TLC plates with chloroform as the eluent. As shown in Fig. 2, for the BODIPY physically encapsulated nanoparticles (compound **5**, Fig. 2A), there is a green fluorescent spot on the top of the TLC plate, whereas there is no moving fluorescent spot for the one with the covalently-encapsulated dye **1** (Fig. 2B). The same phenomenon was observed for nanoparticles encapsulated with the dye pair of compound **8** and dye **2** (Fig. 2C,D). The main reason for this phenomenon is that the dyes physically encapsulated in the nanoparticles can easily leak out from the porous silica matrix, dissolve and move together with chloroform. However, for the silylated BODIPY dyes, the dye molecules are covalently linked to the silica matrix and no dye leakage was observed. To further verify this hypothesis, we mixed chloroform with an aqueous nanoparticles solution (volume ratio = 1 : 1) to detect the dispersion of the dyes, as shown in Fig. 3. After stirring for an hour, physically dye-encapsulated nanoparticles (samples 1 and 3) suffered from dye leakage, and dyes partly transferred into the organic phase ($CHCl_3$). Therefore, green or red fluorescence can be observed under UV light excitation. However, dye leakage would not happen for nanoparticles with covalently-encapsulated dyes (samples 2 and 4). As a result, these nanoparticles with covalently-encapsulated dyes exhibit advantages over those with physically-encapsulated dyes in avoiding dye leakage, which will be of great value during *in vivo* circulation of fluorescent probes.

Linear absorption and emission spectra of the nanoparticles with covalently-encapsulated dyes were obtained in water at room temperature and are shown in Fig. 4A. It can be found that the absorption and emission spectra of nanoparticles with covalently-encapsulated dyes are almost the same as their corresponding free dyes, except that the absorption and fluorescence bands of dye **2** became broader after the encapsulation into the silica nanoparticles, which is probably due to its larger molecular size and stronger vibrational coupling of the S_0–S_1 transition in the silica matrix. Nonetheless, it proves that the dye molecules have been successfully encapsulated into the silica nanoparticles. The fluorescence quantum yields of dye **1**–NPs and dye **2**–NPs are about 0.69 and 0.04, respectively. The fluorescence quantum yield of dye **2**–NPs is much lower than that of dye **1**–NPs, which is probably due to the broader absorption band in aqueous solution, thus resulting in the increased self-absorption within the nanoparticles. Similarly, the fluorescence quantum yields of nanoparticles with the physically-encapsulated dye (**5**) and nanoparticles with the physically-encapsulated dye (**8**) are about 0.72 and 0.07, respectively,

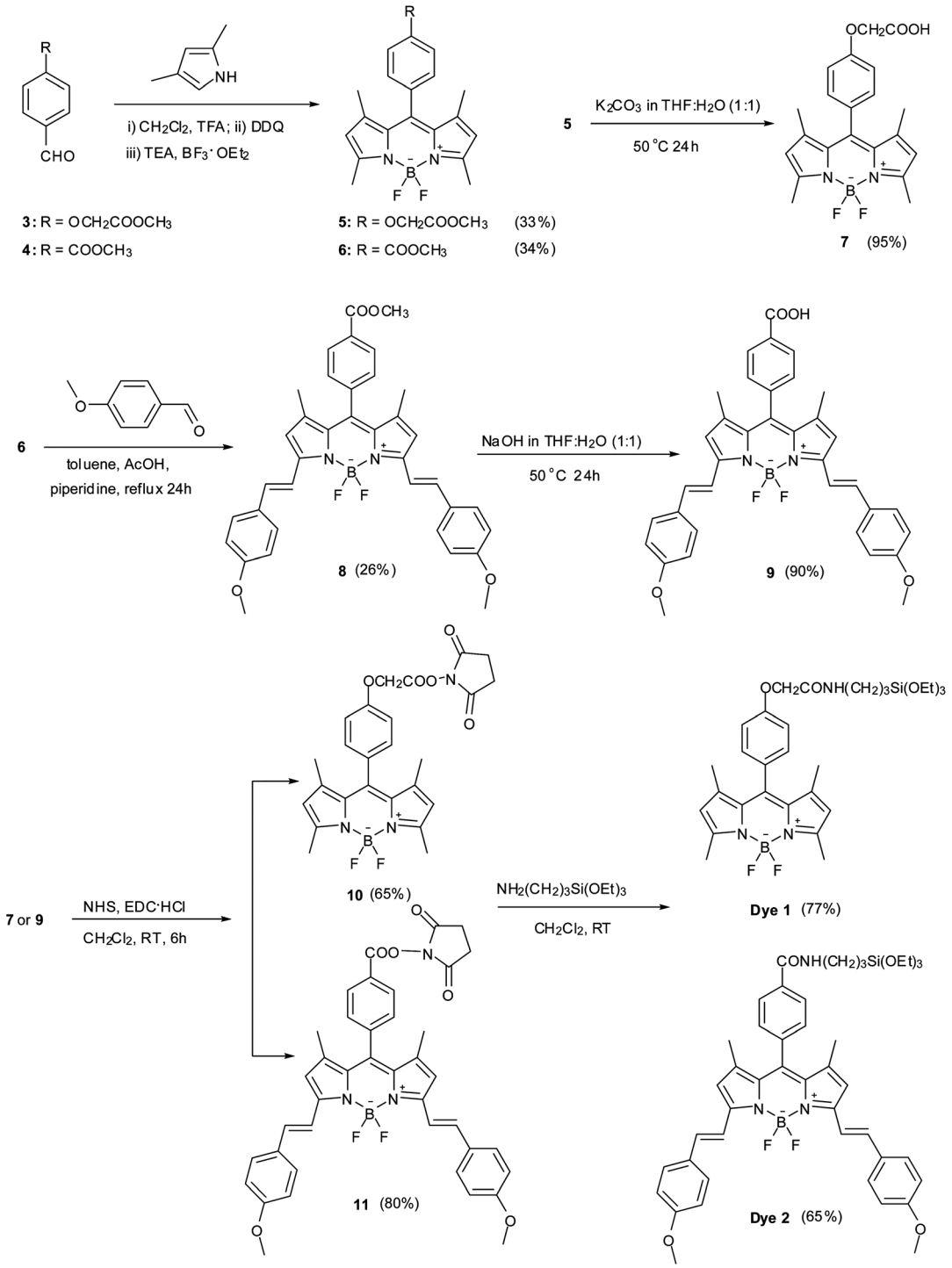

Scheme 1 Synthesis of BODIPY dyes.

which are comparable to that of nanoparticles with the covalently-encapsulated dyes.

It also can be found from Fig. 1 and Fig. 4A that the emission spectrum of dye **1** partially overlaps the absorption spectrum of dye **2**, which is a necessary condition for fluorescence resonance energy transfer (FRET) from dye **1** to dye **2**.[21] To investigate whether the two fluorophores could be co-encapsulated into the same nanoparticles to realize the FRET from dye **1** to dye **2**, we prepared silica nanoparticles containing both dye **1** and dye **2** (dye doping ratio = 1 : 1 by molar ratio). Fig. 4B shows the normalized fluorescence spectra of two sets of nanoparticles by excitation at 488 nm. Fluorescence spectra of (dye **1** + dye **2**)–NPs have two emission peaks located at 513 nm and 665 nm, respectively, which correspond to the emission peaks of dye **1** and dye **2**, respectively. Therefore, both dyes were covalently encapsulated into the same nanoparticle, where the two dyes are

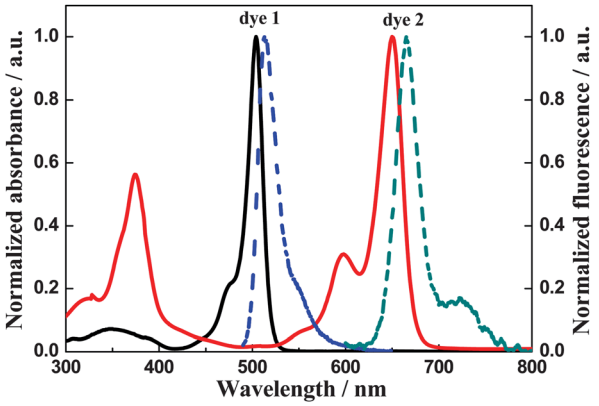

Fig. 1 Normalized linear absorption (—) and emission spectra (---) of dye **1** (excitation: 488 nm) and dye **2** (excitation: 595 nm) in toluene.

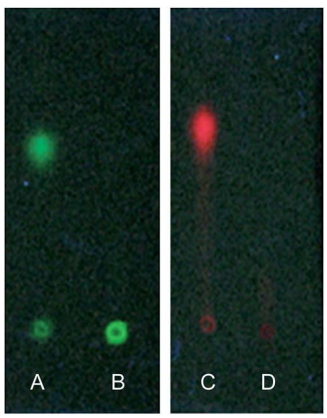

Fig. 2 Pictures of thin layer chromatography (TLC) plates under UV light (365 nm) of nanoparticles with the physically-encapsulated dye (**5**) (A), covalently-encapsulated dye **1** (B), physically-encapsulated dye (**8**) (C) and covalently-encapsulated dye **2** (D).

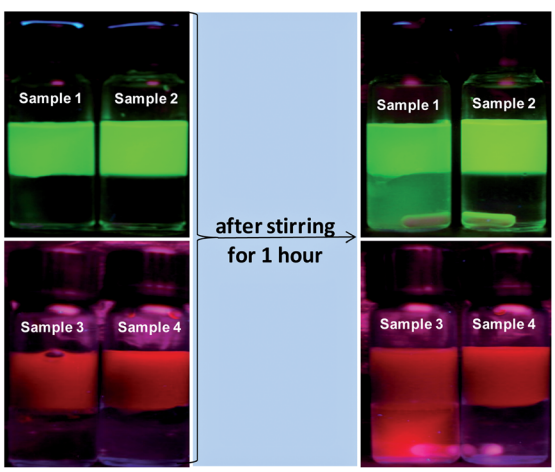

Fig. 3 Pictures of samples 1–4 under UV light (365 nm) excitation before and after stirring for 1 h. Sample 1: nanoparticles with the physically-encapsulated dye (**5**); sample 2: nanoparticles with the covalently-encapsulated dye **1**; sample 3: nanoparticles with the physically-encapsulated dye (**8**) and sample 4: nanoparticles with the covalently-encapsulated dye **2**.

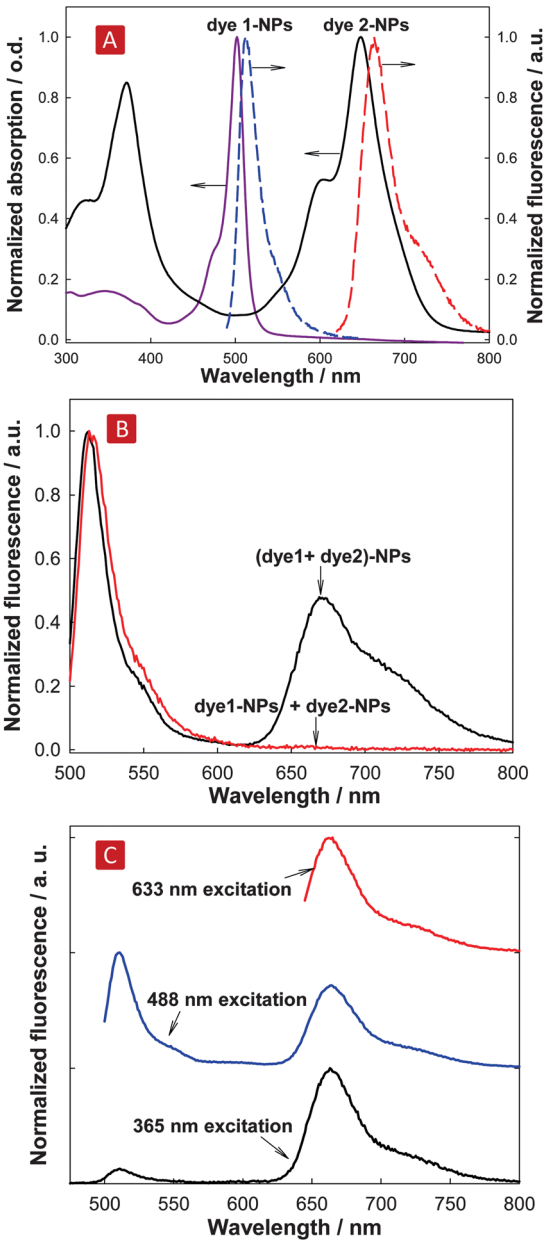

Fig. 4 Normalized linear absorption (—) and emission spectra (---) of (A) nanoparticles with covalently-encapsulated dyes in water (dye **1**–NPs were excited at 488 nm; dye **2**–NPs were excited at 595 nm); (B) normalized emission spectra (excited at 488 nm) of NPs with the covalently-encapsulated (dye **1** + dye **2**) and a mixture of NPs with the covalently-encapsulated dye **1** + NPs with the covalently-encapsulated dye **2** in water; and (C) emission spectra of NPs with the covalently-encapsulated (dye **1** + dye **2**) excited by light at different wavelengths: 365 nm, 488 nm, 633 nm.

in a proximity (1–10 nm) for efficient FRET. We also measured the fluorescence spectrum of the physical mixture of dye **1**–NPs and dye **2**–NPs (mixture ratio = 1 : 1 by molar ratio), and found that there is no emission for dye **2** (Fig. 4B). The reason for this phenomenon is that dye **2** and dye **1** are in a proximity of >20 nm in this case, and no FRET can take place. Therefore, (dye **1** + dye **2**)–NPs exhibit a dramatically increased long-wavelength emission compared to the physical mixture of dye **1**–NPs and dye

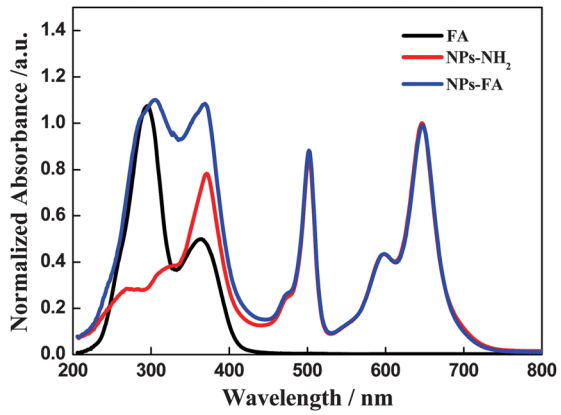

Fig. 5 Normalized absorbance of free folic acid (FA), amino-terminated nanoparticles (NPs–NH_2) and FA conjugated nanoparticles (NPs–FA) in water.

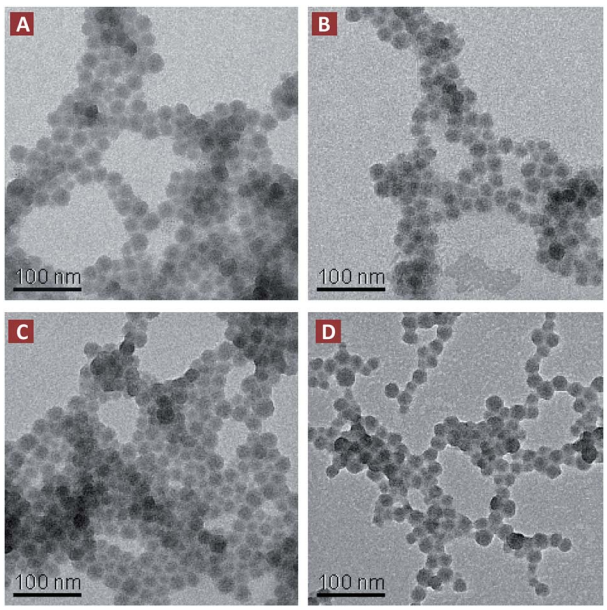

Fig. 6 TEM images of silica nanoparticles (A) nanoparticles with the covalently-encapsulated dye **2**, (B) nanoparticles with the physically-encapsulated dye (**8**), (C) nanoparticles with the covalently-encapsulated (dye **1** + dye **2**) and (D) nanoparticles with the covalently-encapsulated (dye **1** + dye **2**) and FA-conjugated nanoparticles.

2–NPs. The emission color of the nanoparticles from green to red can be controlled by adjusting the doping ratio of the two dyes. On the other hand, the change in excitation wavelength leads to the change in fluorescence spectra as shown in Fig. 4C, which is useful for multiplex imaging or bioarray applications. These dual-dye-doped nanoparticles are able to circumvent one of the shortcomings of BODIPY dyes, *i.e.* small Stokes shifts.

In order to selectively target folate receptors, which are over-expressed in several kinds of human cancer cells, such as breast, ovarian, kidney and prostate cancer cells, the surfaces of the nanoparticles were functionalized with FA. The successful conjugation of FA to the nanoparticles was confirmed by UV-vis absorption spectra. By comparing the absorption spectra of free FA, amino-terminated particles (NPs–NH_2) and FA-modified

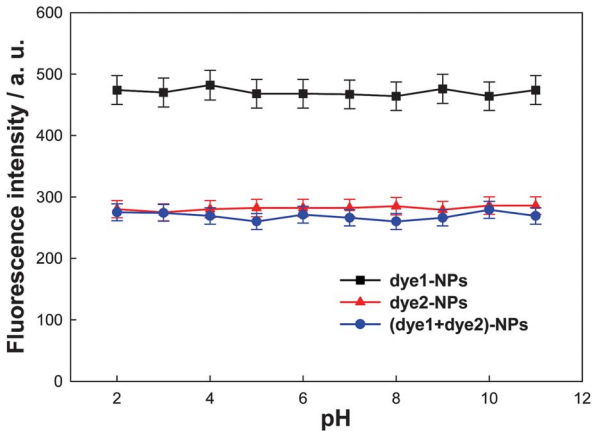

Fig. 7 Effect of pH on the intensity at the fluorescence maximum of the nanoparticles: NPs with the covalently-encapsulated dye **1** (■, excitation at 488 nm, emission at 517 nm), NPs with the covalently-encapsulated dye **2** (▲, excitation at 633 nm, emission at 667 nm) and NPs with the covalently-encapsulated (dye **1** + dye **2**) (●, excitation at 488 nm, emission at 517 nm).

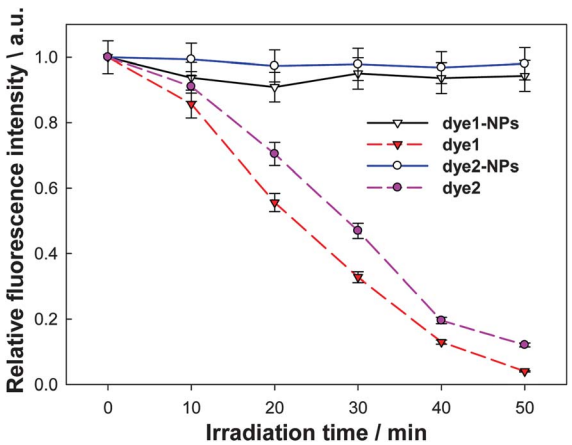

Fig. 8 Photobleaching behaviours of nanoparticles with the covalently-encapsulated dye **1** (or dye **2**) *versus* free dyes (the curves are normalized at their peaks).

particles (NPs–FA), in Fig. 5, we can find that the absorption spectrum of NPs–FA is quite similar to that of NPs–NH_2 except for the expected absorption peak at 290 nm, which is the characteristic absorption peak of FA. Furthermore, the spectra of NPs–FA and free FA have similar absorption peaks at around 290 nm. Thus, FA was believed to have been successfully conjugated to the surfaces of nanoparticles. It should be noted that the surfaces of these nanoparticles can be further tailor-made according to the particular biological applications.

The synthesized silica nanoparticles were characterized in terms of size and morphology by transmission electron microscopy (TEM). The TEM images reveal that most of the nanoparticles are spherical in shape and monodisperse with diameters ranging from 20 to 25 nm. It was observed that the morphology and the size of the nanoparticles with the covalently-encapsulated dye (**2**) and those with the physically-encapsulated dye (**8**) are almost identical (Fig. 6A and B). Fig. 6C shows the morphology of dual-dye-doped nanoparticles, which is also

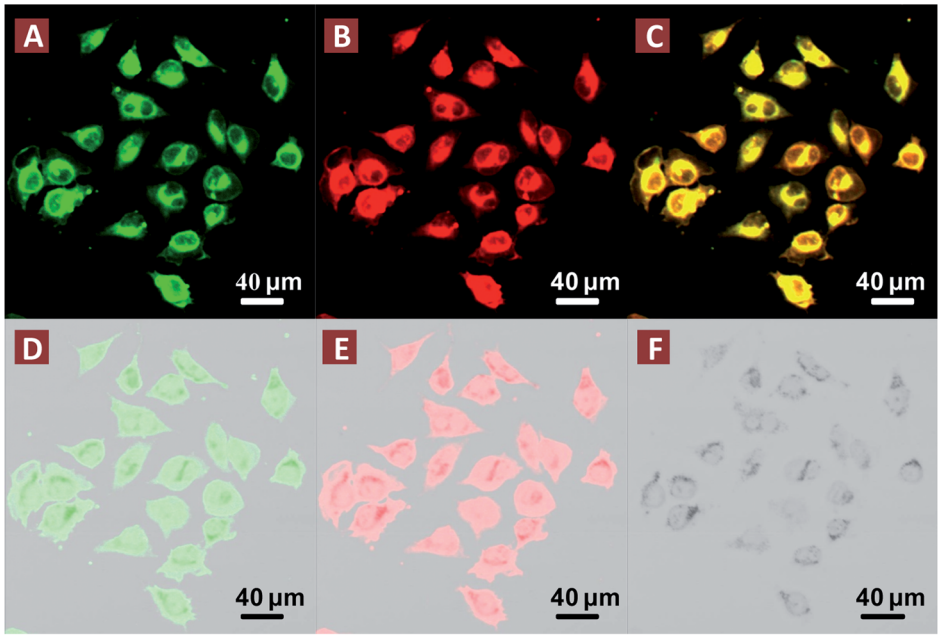

Fig. 9 Confocal microscopic images of HeLa cells treated with dual-dye-doped nanoparticles: (A) excited at 488 nm, (B) excited at 633 nm, (C) merger of (A) and (B), (D and E) the overlays of fluorescence and transmission images and (F) transmission image.

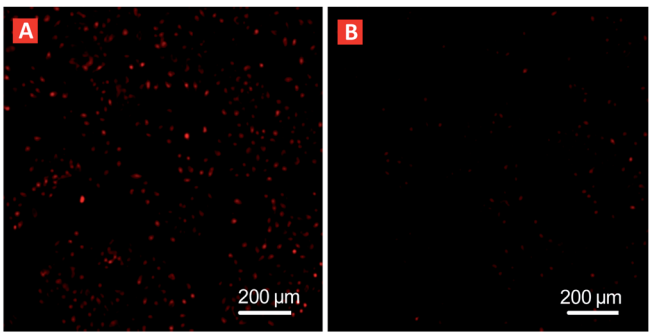

Fig. 10 Images of HeLa cells incubated with NPs–FA: (A) without free folic acid pretreatment and (B) with free folic acid pretreatment.

similar to the nanoparticles with a single dye covalently-encapsulated (Fig. 6A). After the surface modification with FA, the size of nanoparticles did not change except for slight aggregation as shown in Fig. 6D. The size of these nanoparticles is small enough to extend the circulation time of the particles in organisms, and thus increase the accumulation of the particles in the targeted tumor.[22]

In order to be effectively applied to complex physiological environments, in some cases it is important to keep the fluorescence property of the nanoparticles stable over a range of pH values. Fig. 7 describes the effect of pH on the intensity at the nanoparticle fluorescence maximum. From the figure, we can clearly find that over the pH range from 2 to 11, the fluorescence intensity of dye **1**–NPs, dye **2**–NPs and (dye **1** + dye **2**)–NPs were around 475 ± 14, 281 ± 8 and 267 ± 8, in that order. Altering the pH value has almost no influence on the emission intensity of the nanoparticles, which confirmed their suitability for biological applications. These results also showed that the dye-encapsulated nanoparticles have less sensitivity of emission to environments due to their decreased interactions with the environments.

The photostability for the nanoparticles is also important when they are used as fluorescent markers in complex physiological environments. Fig. 8 shows the photobleaching behavior of the nanoparticles with the covalently-encapsulated dyes and the free dyes. As expected, after exposure to light irradiation (365 nm, 1 mW cm^{-2}) for 50 min, the dye-encapsulated nanoparticles (dye **1**–NPs or dye **2**–NPs) show reduced photobleaching compared to the free dye molecules (dye **1** or dye **2**). The photobleaching is known to be dependent on the solvent interactions and is related to a bimolecular reaction between the dyes and reactive species, such as oxygen.[17] The silica framework provides protection for the encapsulated dyes by making them inaccessible to the solvent, which results in increased photostability for the dye-encapsulated nanoparticles. At the same time, a thick layer of the silica coating may also contribute to the enhanced photostability by preventing oxygen molecule penetration into the nanoparticles to react with the dye molecules. This mechanism for higher photostability for silica nanoparticles is different from that observed for gold nanoparticles, where their enhanced fluorescence is mainly caused by plasmonic interactions between the nanoparticles and fluorophores.[23] It is worth mentioning that silica nanoparticles used in this study may also be synthesized on the core of gold nanoparticles to obtain novel hybrid nanoparticles with increased photostability/durability.

Cellular imaging

To investigate the feasibility of fluorescence nanoparticles for biomedical imaging, HeLa cells were treated with the dual-dye-doped nanoparticles. The sample exhibits multi-color emission when excited by light with different wavelengths. Fig. 9A and Fig. 9B show the confocal microscopy images of HeLa cells stained with nanoparticles excited at 488 nm and 633 nm,

respectively. Fig. 9C was the merged image of Fig. 9A and B. Fig. 9F shows the corresponding transmission images, and Fig. 9D and E are the overlays of the corresponding fluorescence images and the transmission image. These images clearly illustrate the successful internalization of nanoparticles by the HeLa cells. These images also suggest the location of the probe in the cytoplasm of the living HeLa cells. At the same time, we did not observe any signs of morphological damage to the cells upon treatment with these nanoparticles for 1–2 h, which demonstrates their negligible toxicity. As shown herein, changing the excitation wavelength, we can conveniently switch the emitting color to avoid the background emission. With FRET within the dual-dye-doped nanoparticles, the light from the emission and the excitation can be separated easily. In addition, it was demonstrated again that two different dyes were successfully encapsulated into the same nanoparticles. Based on these, nanoparticles with dual emission characteristics would be an excellent material for live cell imaging and multiplexed bioassay.

Targeting ability of FA-functionalized nanoparticles

Next, in order to verify the feasibility of FA-functionalized nanoparticles for cancer cell targeting applications, HeLa cells were used as model cancer cells because they over-express the folate receptors.[22,24] A standard competitive inhibition assay was performed to validate that the delivery of nanoparticles to HeLa cells was mediated *via* the folate receptors. In this array, HeLa cells were cultured in FA-functionalized nanoparticles medium with or without free FA addition. The uptake of NPs–FA to HeLa cells was visualized by confocal microscopy *in vitro* conditions. As shown by the fluorescence microscopy images in Fig. 10A, a bright fluorescence signal was observed from the cells without being pretreated with FA. In contrast, a much weaker signal was obtained from those being blocked with FA, showing that the cellular uptake of the nanoparticles was enhanced by conjugating FA molecules to them rather than the non-specific binding between the nanoparticles and HeLa cells. This result was consistent with previous studies on the folate receptor-dependent cellular uptake of FA-conjugated nanoparticles.[24] Again, it also proves the successful conjugation of FA to the nanoparticles. It should be noted that with the amino groups on the nanoparticle surface, the nanoparticles can also be further functionalized to achieve some other desired diagnostic and therapeutic purposes by conjugation with antibodies or drugs.[25]

Conclusions

In conclusion, we have successfully synthesized and characterized two silylated BODIPY derivatives, which are covalently incorporated into amorphous silica nanoparticles using a normal micellar method, leading to the formation of hybrid organic/inorganic nanoparticles with diameters ranging from 20 to 25 nm. Compared to nanoparticles with the physically-encapsulated dyes, those with the covalently-encapsulated dyes are free of any dye leakage. At the same time, the dye-encapsulated nanoparticles (dye **1**–NPs or dye **2**–NPs) show reduced photobleaching compared to the free dye molecules (dye **1** or dye **2**). The dual-dye-doped nanoparticles are facilely prepared by using two silylated BODIPY derivatives with different absorption and emission spectra. Due to the overlap between the emission spectrum of dye **1** and absorption spectrum of dye **2**, FRET was achieved in these dual-dye-doped nanoparticles, thus resulting in dual emission of the nanoparticles. For the dual-dye-doped nanoparticles, two-color imaging was demonstrated with a minimal background signal by employing an appropriate excitation light source and appropriate excitation/emission filter sets. In addition, these nanoparticles show less sensitivity of emission to the environment, which is advantageous for some biological applications. Further, the dual-dye-doped nanoparticles were functionalized with FA and their selective targeting to tumor cells was realized. The results indicated that these nanoparticles would be good candidates for live cell imaging and other biomedical applications.

Experimental

Materials and instruments

All chemicals were purchased from Aladin (China) and Aldrich and were used without further purification. All solvents used here were analytical grade and used as received. ^{1}H NMR (400 MHz) was recorded on a Bruker AVANCE 400 spectrometer. Mass spectra were obtained from the Shanghai Mass Spectrometry Center, Shanghai Institute of Organic Chemistry, CAS, China. Fluorescence imaging of HeLa cells was recorded by confocal microscopy (FV 1000, Olympus) with a 10×microscope objective. A He–Ne laser (632.8 nm) and an Argon ion laser (488 nm) were used for excitation.

Synthesis of compound 5

The synthesis of compound **5** was similar to that described previously.[9] Briefly, benzaldehyde (5.0 mmol) and 2,4-dimethylpyrrole (10.2 mmol) were dissolved in dry CH_2Cl_2 (250 mL) under a nitrogen atmosphere. One drop of TFA was added and the solution was stirred overnight at room temperature. Then, a solution of DDQ (5.1 mmol) in CH_2Cl_2 was added. Triethylamine (7.63 mL) was added to resulting solution, followed by an addition of $BF_3{\cdot}OEt_2$ (7.63 mL). The mixture was stirred for another 40 min, then it was washed with water. The aqueous solution was extracted with CH_2Cl_2, and the organic fractions were dried over $MgSO_4$, filtered, and the solvent evaporated under reduced pressure. The crude product was purified by flash chromatography (silica gel, hexane : CH_2Cl_2 = 1 : 2 by vol) to afford compound **5** (0.686 g, 33%). ^{1}H NMR (400 MHz, $CDCl_3$, 25 °C, TMS): δ = 7.23 (d, J = 8.8 Hz, 2H), 7.03 (d, J = 8.8 Hz, 2H), 5.97 (s, 2H), 4.70 (s, 2H), 3.83 (s, 3H), 2.55 (s, 6H), 1.41 ppm (s, 6H).

Synthesis of compound 7

Compound **5** (0.4 g, 0.97 mmol) and potassium carbonate (0.40 g, 2.91 mmol) were dissolved in THF : water (50 mL : 50 mL) and stirred for 24 h at 50 °C. After cooling, the mixture was acidified until pH = 3–4 by adding a 10% (v/v) aqueous solution of hydrochloric acid. The crude mixture was extracted three times with CH_2Cl_2. The combined organic phases were dried over $MgSO_4$ and the solvent was distilled off under reduced pressure to afford compound **7** (0.35 g, 95%). ^{1}H NMR (400 MHz, $CDCl_3$,

25 °C, TMS): $\delta = 7.15$ (d, $J = 8.8$ Hz, 2H), 7.03 (d, $J = 8.8$ Hz, 2H), 5.97 (s, 2H), 4.48 (s, 2H), 2.55 (s, 6H), 1.41 ppm (s, 6H).

Synthesis of compound 10

Under a nitrogen atmosphere, a dichloromethane solution of compound **7** (0.3 g, 0.79 mmol), NHS (0.27 g, 2.37 mmol) and 1-ethyl-3-(3-dimethylaminopropyl)carbodiimide hydrochloride (EDC·HCl) (0.45 g, 2.37 mmol) was stirred for 4 h at room temperature. After completion of the reaction, the mixture were quenched with a saturated ammonium chloride solution and extracted with CH_2Cl_2. The organic phase was dried over $MgSO_4$ and distilled off under reduced pressure. The crude product was purified by column chromatography (silica gel, diethyl ether : hexane = 1 : 1 by vol) to afford compound **10** (0.25 g, 65%) as a red-orange solid. ^{1}H NMR (400 MHz, $CDCl_3$, 25 °C, TMS): $\delta = 7.23$ (d, $J = 8.8$ Hz, 2H), 7.08 (d, $J = 8.8$ Hz, 2H), 5.97(s, 2H), 5.04 (s, 2H), 2.88 (brs, 4H), 2.55 (s, 6H), 1.41 ppm (s, 6H); HRMS: *m*/*z*: calcd for $C_{26}H_{27}BF_2N_3O_5$: 495.1777; found: 495.1810.

Synthesis of dye 1

To a solution of compound **10** (0.1 g, 0.2 mmol) in CH_2Cl_2 (5 mL) was added APTES (0.13 g, 0.6 mmol). The resulting reaction mixture was stirred overnight at room temperature under nitrogen atmosphere. Solvent was evaporated under reduced pressure and the mixture was purified by column chromatography (silica gel, diethyl ether : hexane = 1 : 1 by vol) to afford dye **1** (0.09 g, 77%). ^{1}H NMR (400 MHz, $CDCl_3$, 25 °C, TMS): $\delta = 7.23$ (d, $J = 8.4$ Hz, 2H), 7.04 (d, $J = 8.4$ Hz, 2H), 5.98 (s, 2H), 4.54 (s, 2H), 3.83 (q, $J = 7.2$ Hz, 6H), 3.38 (q, $J = 6.8$ Hz, 2H), 2.55 (s, 6H), 1.72–1.65 (m, 2H), 1.412 (s, 6H), 1.23 (t, $J = 7.2$ Hz, 9H), 0.657 ppm (t, $J = 0.8.0$ Hz, 2H); HRMS: *m*/*z*: calcd for $C_{30}H_{42}BF_2N_3O_5Si$: 601.2955; found: 601.2986; elemental analysis calcd (%) for $C_{30}H_{42}BF_2N_3O_5Si$: C 59.90, H 7.04, N 6.99; found: C 59.56, H 7.03, N 6.81.

Synthesis of compound 6

The synthesis of compound **6**[26] was similar to that of compound **5**. A red crystalline solid (1.2 g, 34%). ^{1}H NMR (400 MHz, $CDCl_3$, 25 °C, TMS): $\delta = 8.18$ (d, $J = 8.4$ Hz, 2H), 7.41 (d, $J = 8.4$ Hz, 2H), 5.97 (s, 2H), 3.97 (s, 3H), 2.56 (s, 6H), 1.36 ppm (s, 6H).

Synthesis of compound 8

Compound **6** (0.8 g, 2.09 mmol) and *p*-methoxybenzaldehyde (0.63 g, 4.60 mmol) were added to a mixture of toluene, acetic acid (0.7 mL) and piperidine (0.8 mL). The water formed during the reaction was removed azeotropically by heating the mixture in a Dean–Stark apparatus for 24 h. The solution containing the crude product was concentrated under reduced pressure and purified by silica gel column chromatography ($CHCl_3$: hexane = 2 : 1 by vol) to afford compound **8** (0.34 g, 26%). ^{1}H NMR (400 MHz, $CDCl_3$, 25 °C, TMS): $\delta = 8.19$ (d, $J = 8.0$ Hz, 2H), 7.61 (d, $J = 16.0$ Hz, 2H), 7.59 (d, $J = 8.8$ Hz, 4H), 7.46 (d, $J = 8.0$ Hz, 2H), 7.22 (d, $J = 16.0$ Hz, 2H), 6.94 (d, $J = 8.8$ Hz, 4H), 6.62 (s, 2H), 3.92 (s, 3H), 3.86 (s, 6H), 1.42 ppm (s, 6H); HRMS: *m*/*z*: calcd for $C_{37}H_{33}BF_2N_2O_4$: 618.2501; found: 618.2532.

Synthesis of compound 9

The synthesis of compound **9** was similar to that of compound **7** except for the replacement of potassium carbonate with sodium hydroxide. The mixture was heated at 50 °C for 24 h. The product was obtained as a dark blue crystalline solid (0.176 g, 90%). ^{1}H NMR (400 MHz, DMSO-D_6, 25 °C, TMS): $\delta = 8.09$ (d, $J = 8.0$ Hz, 2H), 7.57 (d, $J = 17.2$ Hz, 2H), 7.56 (d, $J = 6.8$ Hz, 4H), 7.55 (d, $J = 8.0$ Hz, 2H), 7.38 (d, $J = 17.2$ Hz, 2H), 7.02 ($J = 6.8$ Hz, 4H), 6.98 (s, 2H), 3.89 (s, 6H), 1.37 ppm (s, 6H); HRMS: *m*/*z*: calcd for $C_{36}H_{31}BF_2N_2O_4$: 604.2345; found: 604.2376.

Synthesis of compound 11

The synthesis of compound **11** was similar to that of compound **10**. The product was obtained by precipitation from methanol as a dark blue crystalline solid (0.139 g, 80%). ^{1}H NMR (400 MHz, $CDCl_3$, 25 °C, TMS): $\delta = 8.28$ (d, $J = 8.4$ Hz, 2H), 7.61 (d, $J = 16.0$ Hz, 2H), 7.60 (d, $J = 8.4$ Hz, 4H), 7.56 (d, $J = 8.4$ Hz, 2H), 7.24 (d, $J = 16.0$ Hz, 2H), 6.94 (d, $J = 8.4$ Hz, 2H), 6.64 (s, 2H), 3.86 (s, 6H), 2.96 (brs, 4H), 1.44 ppm (s, 6H); HRMS: *m*/*z*: calcd for $C_{40}H_{34}BF_2N_3O_6$: 701.2509; found: 701.2540.

Synthesis of dye 2

The synthesis of dye **2** was similar to that of dye **1**. A dark blue crystalline solid (65% yield). ^{1}H NMR (400 MHz, $CDCl_3$, 25 °C, TMS): $\delta = 7.95$ (d, $J = 8.0$ Hz, 2H), 7.61 (d, $J = 16.0$ Hz, 2H), 7.59 (d, $J = 8.8$ Hz, 4H), 7.44 (d, $J = 8.0$ Hz, 2H), 7.22 (d, $J = 16.0$ Hz, 2H), 6.94 (d, $J = 8.8$ Hz, 4H), 6.69 (s, 2H), 3.86 (s, 6H), 3.85 (q, $J = 7.2$ Hz, 6H), 3.53 (q, $J = 6.8$ Hz, 2H), 1.85–1.78 (m, 2H), 1.42 (s, 6H), 1.24 (t, $J = 6.8$ Hz, 9H), 0.76 ppm (t, $J = 8.0$ Hz, 2H); HRMS: *m*/*z*: calcd for $C_{45}H_{52}BF_2N_3O_6Si$: 807.3686; found: 807.3717; elemental analysis calcd (%) for $C_{45}H_{52}BF_2N_3O_6Si$: C 66.91, H 6.49, N 5.20; found: C 66.74, H 6.57, N 5.12.

Synthesis of BODIPY-covalently incorporated amine-terminated silica nanoparticles

The nanoparticles were prepared by the hydrolysis and polycondensation of the organotrialkoxysilane precursors within the non-polar core of an oil-in-water microemulsion.[27] Briefly, to 10 mL of 2% aqueous docusate sodium (AOT) solution, 300 μL of co-surfactant 1-butanol and 100 μL of *N*-methyl-2-pyrrolidone (NMP) were added with stirring, to form an oil-in-water microemulsion. To this microemulsion, 100 μL of NMP solution containing individual silylated BODIPY dyes (or a mixture of dye **1** and dye **2**) (10 mM) was added, followed by an addition of 100 μL of VTES, and the resulting mixture was stirred for an hour, then the polymerization reaction was initialized by an addition of 10 μL of APTES. The solution was further stirred at room temperature overnight. Next, the surfactant, co-surfactant and other unreacted molecules were removed by dialysis using a cellulose membrane. After dialysis, the nanoparticles were sterile filtered and stored at 4 °C for future use. The dye-encapsulated nanoparticles used as a control were synthesized by the same way

mentioned above except for the replacement of dye **1** with compound **5**, and dye **2** with compound **8**, respectively.

Surface modification of amine-terminated silica nanoparticles with FA

For this purpose, esterification of folic acid with NHS in dry dimethyl sulfoxide (DMSO) in the presence of EDC·HCl and triethylamine as catalyst was prepared as reported in the literature.[28] Then, to 10 mL of the nanoparticles suspension (pH adjusted to 9.0 using sodium carbonate/sodium bicarbonate buffer solution), 5 mg of folic acid *N*-hydroxysuccinimidyl ester (FA–NHS) in 100 μL DMSO was added, and the mixture was stirred at room temperature for 5 h. To separate the folic-conjugated nanoparticles from unreacted FA–NHS and other by-products, the mixture was dialyzed against deionized water for 48 h. Finally, all the samples were filtered through a 0.22 μm cutoff membrane filter and stored at 4 °C for further use.

Linear optical properties and fluorescence quantum yields

The linear absorption and fluorescence spectra of free dyes and nanoparticles at room temperature were obtained by using a spectrophotometer (Lambda 35 UV/vis) and a Cary Eclipse spectrophotometer, respectively. The fluorescence spectra were collected at 1.0 nm resolution, 0.5 s integration time and 1.0 nm band pass. The relative fluorescence quantum yields of dye **1** and dye **1**–NPs were obtained by comparing the area under the corrected emission spectrum of test sample with that of a solution of Rhodamine 6G ($\Phi = 0.94$ in methanol).[29] The relative quantum yields of dye **2** and dye **2**–NPs were obtained by using cresyl violet ($\Phi = 0.54$ in methanol).[30] For the fluorescence quantum yield measurement experiment, dilute solution with an optical density of <0.25 at the absorption maximum were used. The bioconjugation of the nanoparticles with FA was confirmed by comparing the absorption spectra of free folic acid, unmodified NPs–NH_2 and NPs–FA.

Effect of pH on the emission of nanoparticles

The fluorescence intensities of nanoparticles in different buffer solutions over the pH range from 2 to 11 were measured at their maximum emission wavelengths to evaluate the influence of the pH on the nanoparticles.

Photostability of nanoparticles

For the photobleaching experiment, all the samples are irradiated with 365 nm UV light at an intensity of 1 mW cm^{-2}. The peak emission (515 nm) of dye **1**–NPs and dye **1** are excited at 488 nm, and the peak emission (667 nm) of dye **2**–NPs and dye **2** are obtained with an excitation at 595 nm.

Morphology analysis of nanoparticles

Transmission electron microscopy (TEM) was performed to determine the morphology and size of these nanoparticles by using a JEOL JEM-2010 Transmission Electron Microscope at an accelerating voltage of 80 kV. A drop of nanoparticles suspension solution was placed on a holey carbon film copper grid and left to evaporate.

Culture of HeLa cells

HeLa cells were purchased from Nanjing KeyGen Biotech Co., Ltd. and cultured in medium (DMEM) under a humidified atmosphere (5% CO_2 plus 95% air) at 37 °C. Media were supplemented with 10% heat-inactivated newborn calf serum (Hangzhou Every Green Organism Engineering Materials Co., Ltd.), and 1% penicillin–streptomycin (Nanjing KeyGen Biotech Co., Ltd.). For fluorescence imaging, HeLa cells were seeded into a culture dish (Corning) and incubated for 24 h. Then the nanoparticle solution was added to the cell culture dish (volume ratio dye solution : culture medium = 1 : 5). After incubating for 1.5 h at 37 °C, the culture media were discarded and the culture dish was washed three times with phosphate-buffered saline (PBS) before the fluorescence imaging experiments. For FA competition experiments, HeLa cells were pre-blocked with 3 mM FA for 2 h prior to the addition of nanoparticles at 37 °C. Before measurements, the culture dishes were washed with PBS three times.

Acknowledgements

This work was in part supported by 100 Talents Programme of The Chinese Academy of Sciences and in part supported by Natural Science Foundation of China (21102144). Z.W. thanks the Foundation for The Excellent Youth Scholars of Southeast University.

References

1 T. G. Pavlopoulos, M. Shah and J. H. Boyer, *Appl. Opt.*, 1988, **27**, 4998–4999.
2 A. Loudet and K. Burgess, *Chem. Rev.*, 2007, **107**, 4891–4932.
3 G. Ulrich, R. Ziessel and A. Harriman, *Angew. Chem., Int. Ed.*, 2008, **47**, 1184–1201.
4 J. Karolin, L. B. A. Johansson, L. Strandberg and T. Ny, *J. Am. Chem. Soc.*, 1994, **116**, 7801–7806.
5 H. Sunahara, Y. Urano, H. Kojima and T. Nagano, *J. Am. Chem. Soc.*, 2007, **129**, 5597–5604.
6 H. Kobayashi, M. Ogawa, R. Alford, P. L. Choyke and Y. Urano, *Chem. Rev.*, 2010, **110**, 2620–2640.
7 O. Buyukcakir, O. A. Bozdemir, S. Kolemen, S. Erbas and E. U. Akkaya, *Org. Lett.*, 2009, **11**, 4644–4647.
8 S. Zhu, J. Zhang, G. Vegesna, F.-T. Luo, S. A. Green and H. Liu, *Org. Lett.*, 2011, **13**, 438–441.
9 Q. Zheng, G. Xu and P. N. Prasad, *Chem.–Eur. J.*, 2008, **14**, 5812–5819.
10 R. Ciriminna, M. Sciortino, G. Alonzo, A. d. Schrijver and M. Pagliaro, *Chem. Rev.*, 2011, **111**, 765–789.
11 A. Palma, L. A. Alvarez, D. Scholz, D. O. Frimannsson, M. Grossi, S. J. Quinn and D. F. O'Shea, *J. Am. Chem. Soc.*, 2011, **133**, 19618–19621.
12 R. I. Nooney, C. M. N. McCahey, O. Stranik, X. Le Guevel, C. McDonagh and B. D. MacCraith, *Anal. Bioanal. Chem.*, 2009, **393**, 1143–1149.
13 H. Ow, D. R. Larson, M. Srivastava, B. A. Baird, W. W. Webb and U. Wiesner, *Nano Lett.*, 2005, **5**, 113–117.
14 S. Santra, P. Zhang, K. Wang, R. Tapec and W. Tan, *Anal. Chem.*, 2001, **73**, 4988–4993.
15 J. O. Koskinen, J. Vaarno, N. J. Meltola, J. T. Soini, P. E. Hanninen, J. Luotola, M. E. Waris and A. E. Soini, *Anal. Biochem.*, 2004, **328**, 210–218.
16 L. Wang, C. Yang and W. Tan, *Nano Lett.*, 2005, **5**, 37–43; L. Wang and W. Tan, *Nano Lett.*, 2006, **6**, 84–88.

17 H. Ow, D. R. Larson, M. Srivastava, B. A. Baird, W. W. Webb and U. Wiesner, *Nano Lett.*, 2004, **5**, 113–117.
18 L. Wang, J. Lei and J. Zhang, *Chem. Commun.*, 2009, 2195–2197.
19 H. Y. Lee, D. R. Bae, J. C. Park, H. Song, W. S. Han and J. H. Jung, *Angew. Chem., Int. Ed.*, 2009, **121**, 1265–1269; H. Son, H. Y. Lee, J. M. Lim, D. Kang, W. S. Han, S. S. Lee and J. H. Jung, *Chem.–Eur. J.*, 2010, **16**, 11549–11553.
20 S. Kim, T. Y. Ohulchanskyy, A. Baev and P. N. Prasad, *J. Mater. Chem.*, 2009, **19**, 3181–3188.
21 P. Wu and L. Brand, *Anal. Biochem.*, 1994, **218**, 1–13.
22 S. Mitragotri and J. Lahann, *Nat. Mater.*, 2009, **8**, 15–23.
23 A. Hakonen and N. Strömberg, *Analyst*, 2012, **137**, 315–321; A. Hakonen and N. Strömberg, *Chem. Commun.*, 2011, **47**, 3433–3435.
24 Z. Wang, S. Zong, J. Yang, J. Li and Y. Cui, *Biosens. Bioelectron.*, 2011, **26**, 2883–2889; D. J. Bharali, D. W. Lucey, H. Jayakumar, H. E. Pudavar and P. N. Prasad, *J. Am. Chem. Soc.*, 2005, **127**, 11364–11371.
25 J. M. Rosenholm, A. Meinander, E. Peuhu, R. Niemi, J. E. Eriksson, C. Sahlgren and M. Lindén, *ACS Nano*, 2008, **3**, 197–206; K. Cheng, S. R. Blumen, M. B. MacPherson, J. L. Steinbacher, B. T. Mossman and C. C. Landry, *ACS Appl. Mater. Interfaces*, 2010, **2**, 2489–2495.
26 N. Inoue, Y. Suzuki, K. Yokoyama and I. Karube, *Biosci., Biotechnol., Biochem.*, 2009, **73**, 1215–1217.
27 T. Y. Ohulchanskyy, I. Roy, L. N. Goswami, Y. Chen, E. J. Bergey, R. K. Pandey, A. R. Oseroff and P. N. Prasad, *Nano Lett.*, 2007, **7**, 2835–2842.
28 R. J. Lee and P. S. Low, *J. Biol. Chem.*, 1994, **269**, 3198–3204.
29 W. Baumler and A. Penzkofer, *Chem. Phys.*, 1990, **140**, 75–97.
30 D. Magde, J. H. Brannon, T. L. Cremers and J. Olmsted, *J. Phys. Chem.*, 1979, **83**, 696–699.